Rock and rock mass characterization for deep mining using sonic data

Conference Paper · January 2011

CITATIONS
0

READS
259

3 authors, including:

Benoît Valley
Université de Neuchâtel
120 PUBLICATIONS **1,641** CITATIONS
SEE PROFILE

Robert Bewick
WSP Golder
34 PUBLICATIONS **459** CITATIONS
SEE PROFILE

ARMA 11-371

Rock and rock mass characterization for deep mining using sonic data

Valley, B. & Bewick, R. P.
Geomechanics Research Centre, MIRARCO – Mining Innovation, Sudbury, Ontario, Canada
Hudson, R.
Resolution Copper Company, Superior, Arizona, United States

This paper was prepared for presentation at the 45th US Rock Mechanics / Geomechanics Symposium held in San Francisco, CA, June 26–29, 2011.

ABSTRACT: Rock and rock mass strength characterization is critical for the planning of deep mass mining projects where large capital investments are needed before extraction can begin. The deep nature of such projects also implies that initial data are gathered mostly in and from boreholes, and that core samples can be damaged by high relative stress conditions at the sampling point. In these conditions, it would be advantageous to use wirelogs, like full waveform sonic logs, to assess in situ rock strength and rock mass quality. This paper presents the processing methods that need to be applied to such logs in order to extract relevant sonic parameters and results from correlations between these parameters and rock properties. Literature review as well as the results presented in this paper show that a correlation exists between intact rock strength and p-wave velocity, but large scatter is present when the velocity exceeds about 3.5 km/s. However, sonic velocity is shown to be useful in identifying the occurrence of core damage and potential strength or stress anomalies. The impact of the fracturing level on the sonic response is also studied and is shown to result in increasing attenuation and frequency shift with increases in fracture intensity.

1. INTRODUCTION

Being able to characterize rock and rock masses at early project stages (pre-feasibility, feasibility) – when the ability to influence the design of a mining project is the highest – is critical to manage investor risk for deep mass mining projects. For such projects, where kilometers of development need to be established before ore extraction can begin, initial capital investment is large. For projects of this magnitude, relatively small variations in design parameters such as rock mass strength have large consequences on the project planning, thus increasing investor risk. Also, the deep nature of such projects have two implications: 1) initial data to characterize the rock mass is in most instances solely acquired from boreholes; and 2) relatively high stress conditions have consequences in terms of data acquisition (sample disturbance, e.g. [1, 2, 3]) and rock mass behavior anticipation.

Another important aspect of the rock mass characterization process is the consideration of rock and rock mass property variability. Nowadays, with the implementation of probabilistic approaches, numerical methods allow for the possibility of dealing with variable inputs, enabling uncertainty to be included in the analysis and thus risk to be assessed [e.g. 4]. However, it remains labour intensive to perform an extensive laboratory program that produces a sufficient amount of data to properly characterize the variability of the inputs needed for such analyses.

For these reasons it would be attractive to be able to produce continuous rock property profiles, particularly rock strength profiles, from geophysical logging data. This article reports on preliminary results that aim at using sonic data to better characterize in-situ rock strength and rock mass quality. It focuses primarily on the importance of proper sonic data preprocessing and the results of initial correlations between sonic properties and rock and rock mass properties.

2. RELATATIONSHIPS BETWEEN SONIC & MECHANICAL PROPERTIES OF ROCK

Borehole acoustic logging has broad use in the oil and gas industry to characterize porosity in sedimentary series of relatively weak rock. Applications in hard fractured rocks are not as wide spread, and focused, as this article, on mechanical rock properties including modulus and strength.

The theory of elastic wave propagation in isotropic and homogeneous elastic solids allows relating dynamic elastic properties of rocks to p-wave velocity (Vp) and s-wave velocity (Vs) [e.g. 5]. Also, according to [6], rock

modulus and unconfined compressive strength of rock (*UCS*) are correlated, with typical strength to modulus ratio ranging from 1/200 to 1/500. Thus, one would expect some degree of correlation between rock strength and sonic velocities.

A compilation of published *Vp* and *UCS* data is presented in Fig. 1. [7] measured velocity on core using a portable ultrasonic non-destructive digital indicating tester and derived *UCS* indirectly from Schmidt hammer tests. Their data includes mostly weak sedimentary rocks (sandstone and shales) as well as some igneous and metamorphic rocks. Maximum velocity obtained is 3 km/s for a maximum *UCS* of 72 MPa. For their dataset, they found a strong linear correlation between *Vp* and *UCS* (red line on Fig. 1b). [8] collected strength and velocity data from core samples taken in a complex volcano-clastic sequence. *Vp* was measured on samples and *UCS* was determined directly. Entwisle's data [8] covers *Vp* values from 3.4 to 6.4 km/s and *UCS* values from 5 to 470 MPa. They propose to use an exponential relationship to fit their data. Two other sources, [9] and [10] are included in the database presented in Fig. 1, both are in general agreement with the other data.

Following [8], an exponential function has been fit to the entire dataset. A coefficient of determination (R^2) of 0.63 was obtained. Confidence bounds for 68% and 95% (corresponding to approximately 1 and 2 standard deviation, respectively) were computed and are shown on Fig. 1. The variability in the data increases significantly with increasing velocity, with *Vp* becoming a very uncertain predictor for *UCS* when *Vp* is larger than about 4 km/s. For a velocity of 5 km/s, the data spans a *UCS* range from 20 to 165 MPa, and the 95% confidence bounds suggest that *UCS* could be as low as 12 MPa and as high as 265 MPa. Possibly a better correlation between *Vp* and *UCS* could be obtained if rock types were carefully separated (e.g. differentiate the lithologies in the volcanoclastic series presented by [8]), and failure modes were considered (e.g. include only intact break results from the *UCS* testing).

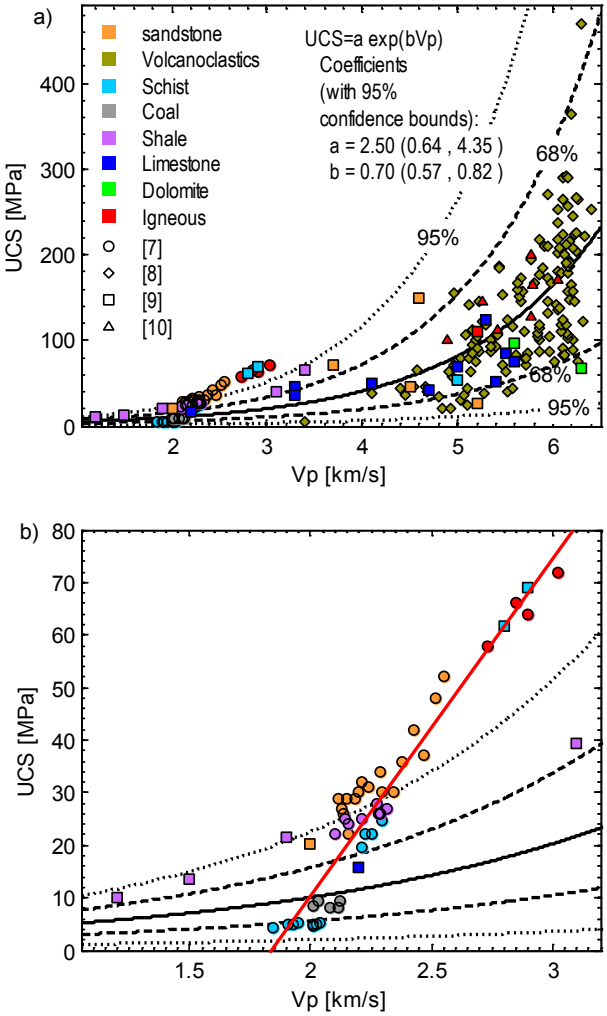

Fig. 1. The relations between *Vp* and *UCS*. Data are compiled from four sources distinguished by symbol shapes. Colours relate to simplified rock type grouping. a) Full range of data with exponential best fit and 68% and 95% confidence range. b) Zoom on the lower velocity range where [7] found a strong linear relationship for their data (red line) that include mostly weak sedimentary rocks.

3. SONIC DATA AND PROCESSING METHODOLOGY

The sonic datasets presented in this paper were acquired in a single borehole, in two runs, one spanning the depth range 1019.0 to 1514.9 m and the other the depth range 1499.3 to 2060.1 m. The dominant lithology is a cretaceous volcanoclastic series (Kvs) affected by predominantly three types of alteration, a phylitic alteration (Kvs-Phy), a propylitic alteration (Kvs-Pro) and an argillic alteration (Kvs-A). The lower 250 m of the borehole are composed of Precambrian quartzites (Qtzite) diabase dykes (Diab-Pro and Diab-Phy), and tertiary intrusions (Ti).

The datasets were acquired using a full wave sonic probe with three receivers from ALT (model FWS50). The receivers are located at a distance of 0.6, 0.8 and 1.0 m from the transmitter. The latter has a central frequency of about 20 kHz. Full waveforms were recorded over 1020 µs at a 4 µs sampling interval, with a depth sampling interval of 0.1 m. Together with the full waveform data, velocity analysis results for *Vp*, *Vs* and *Vst* were supplied. These were obtained using the velocity analysis tool provided in the WellCad© [11] software package. The following discusses the reliability of this analysis and the details of the proper determination of velocity profiles from full wave sonic datasets.

3.1. *Determination of sonic velocity using a semblance analysis*

A common approach to extract velocities from full waveform sonic data is to use a semblance analyses [12]. The semblance analysis is a cross-correlation process that computes the coherence between the waves recorded at each receiver for varying slowness and time lag. When displaying the full waveforms in a time – distance transmitter/receiver plot (Fig. 2), lines in this space will correspond to velocities, with steeper lines equivalent to higher velocities. The coherence between the full waveforms can be evaluated for any velocity (varying slopes in Fig. 2) and any time lag (horizontal shift in Fig. 2). This allows for a semblance plot to be built as presented in Fig. 3, i.e. a display of the coherence between the full waveform in a time lag – slowness (inverse of velocity) space. High coherence will correspond with the velocity of the various modes and their harmonics.

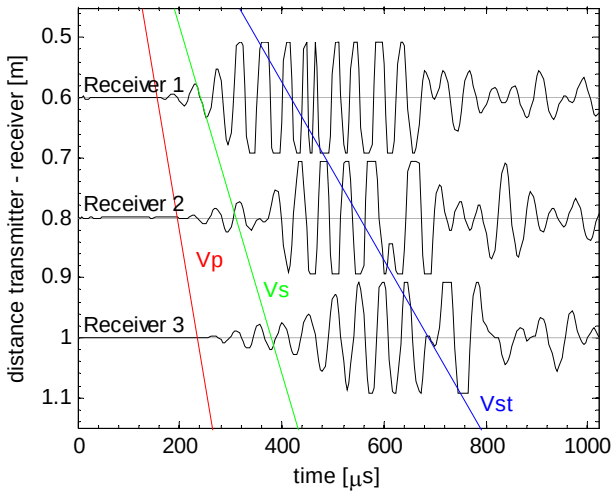

Fig. 2. Example of full waveform data recorded at a depth of 1048.9 m. The waves are displayed in a time – distance receiver space so that lines will correspond to velocities. *Vp*, *Vs* and *Vst* as determined by the semblance processing are also displayed

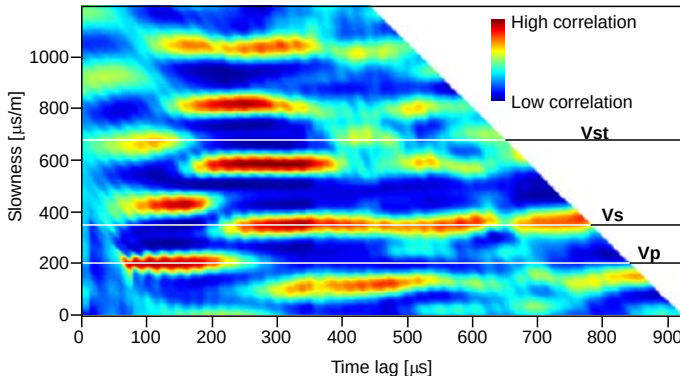

Fig. 3. Semblance analysis results for the data presented in Fig. 2. Slowness is the inverse of velocity. See text for details.

The velocity analysis process implemented in WellCad© is a simplified semblance analysis that reduces the complexity of the analysis by limiting the time lag range for which the analysis is performed and by stacking the results for common slowness. This simplified process speeds up the analysis time, but with the risk of miss evaluating the velocities.

A comparison of the velocities obtained with both techniques, i.e. the full semblance analysis and the reduced semblance analysis, is presented in Fig. 4. The profile obtained with both techniques are very similar for *Vs* and *Vst* (Stoneley wave velocity). However significant discrepancy is already noticeable for *Vp*.

The range of p-wave velocities obtained for each lithology is presented on Fig. 5. The discrepancy between the method is obvious, with the WellCad©

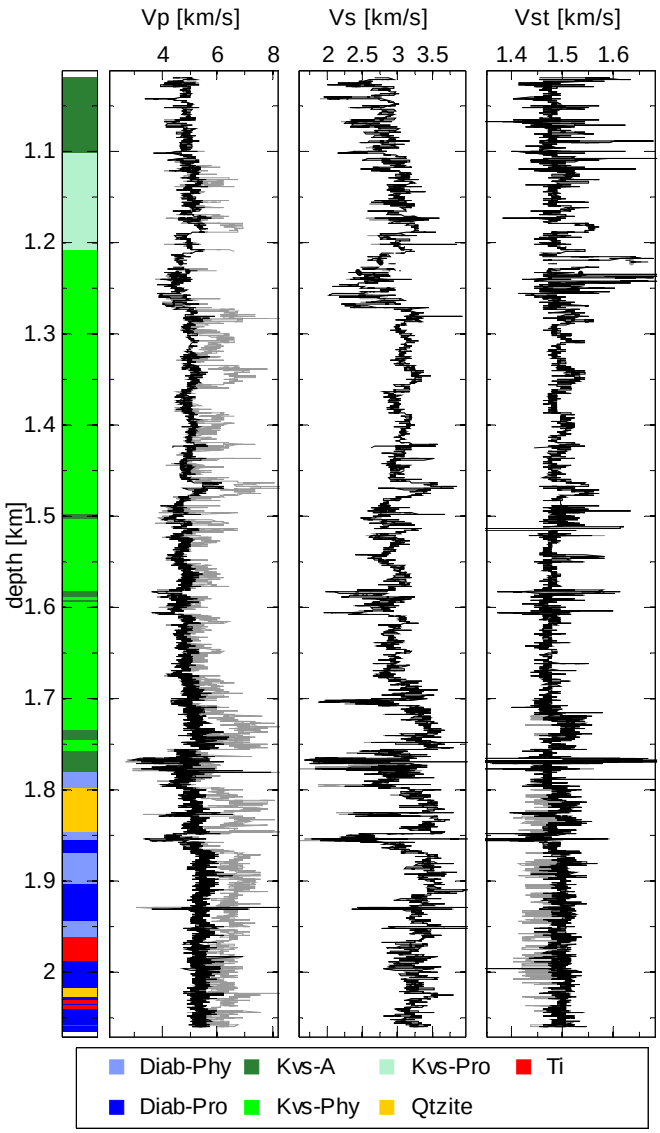

Fig. 4. Velocity profiles, *Vp*, *Vs* and *Vst*, obtained using the full semblance processing (black) and the WellCad© velocity analyses (grey).

results showing generally a significantly higher mean and broader distribution. A discrepancy of more than 1200 m/s in the mean value is observed in one rock unit. The distribution obtained from the WellCad© velocity analysis are bimodal (e.g. Diab-Phy) or with a longer tail towards higher velocities (e.g. Kvs-Phy), suggesting at least partially erroneous velocity determination. Thus, only results from full semblance analysis will be used in the remainder of the paper.

The lithology with the highest velocity is Ti with a mean *Vp* of more than 5.3 km/s. The diabase has a mean *Vp* from 5.2 to 5.3 km/s. The volcano-clastic series has mean velocities ranging from 4.8 to 5.1 km/s with the highest mean velocity for the propylitic alteration type.

3.2. *Extraction of attenuation information*

Sonic attenuation, i.e. the loss of energy over the sonic wave ray path, extraction was attempted from the full waveform data. The approach attempted initially was to compare arrival energy for receivers 2 and 3 with receiver 1, allowing a quantitative attenuation (unit of loss per unit of length) assessment. This approach was found to not be practical with the data because the energy loss between receiver 2 and 3 was not systematic.

Therefore, an alternative approach was used to compute a relative index. The principle of this computation is illustrated in Fig. 6.

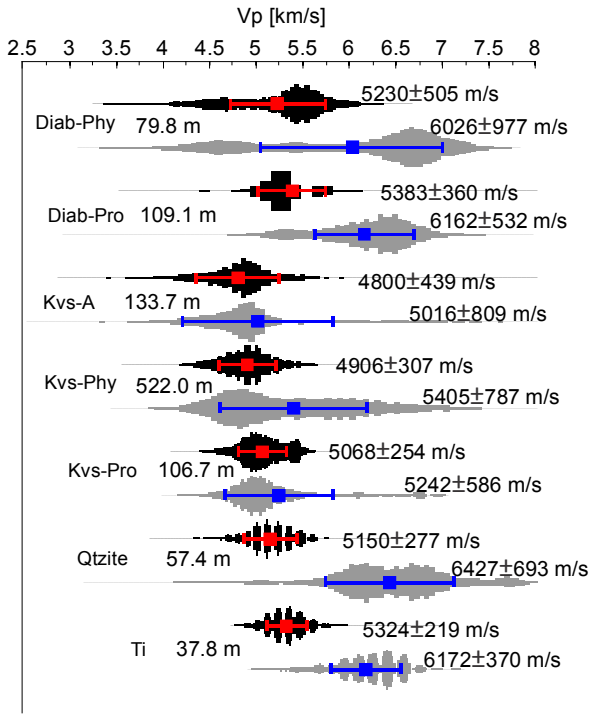

Fig. 5. *Vp* distribution for each lithology together with the mean and 1std (square and error bars). In black and red are the results obtained from the full semblance analyses while in grey and blue are the ones obtained from the WellCad© velocity analysis. Total length, mean±standard deviation values are also indicated.

The first step consisted in re-interpolating the full wave record using a cubic spline interpolant in order to compensate for clipping. Indeed, due to the limited dynamic range of the sonic tool, most of the full waveforms recorded are clipped for the mid-part of the wave. A comparison of the clipped and interpolated wave can be seen on Fig. 6.

The second step was to determine the arrival time for the p-wave, s-wave and Stoneley wave trains. This was achieved by considering that the shortest path is controlled by the critical refraction angle (Snell's law) assuming appropriate tool and borehole geometry, the later using a borehole caliper log, and a sonic velocity in the borehole fluid of 1402 m/s.

The third step was to integrate the waveform for fixed time windows following the computed arrival time (coloured area on Fig. 6). The time windows were chosen to avoid overlap between the p-wave, s-wave and Stoneley wave evaluations, and are 48, 72 and 96 µs respectively.

Finally these results were normalized to the lowest and highest values along the logs. This produced three attenuation indexes, one for the p-wave, the s-wave and the Stoneley wave, ranging from 0 to 1. These data are presented in Fig. 7.

3.3. *Extraction of frequency content information*

The last attribute that was extracted from the full waveform was the median frequency and the power. These were obtained by applying a discrete Fourrier transform to the full wave of the first receiver, previously interpolated to remove clipping. An example of such processing is presented on Fig. 8 for two different depths, one for a typical waveform and the other for an attenuated waveform. The typical dominant

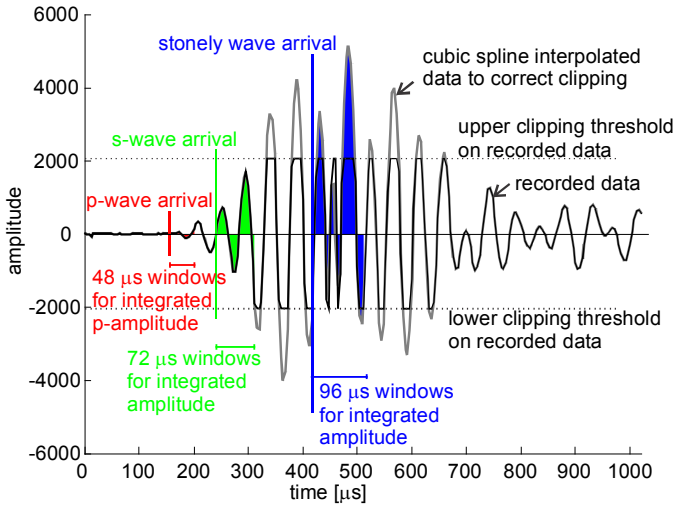

Fig. 6. Principle of computation of relative attenuation index (see text for details).

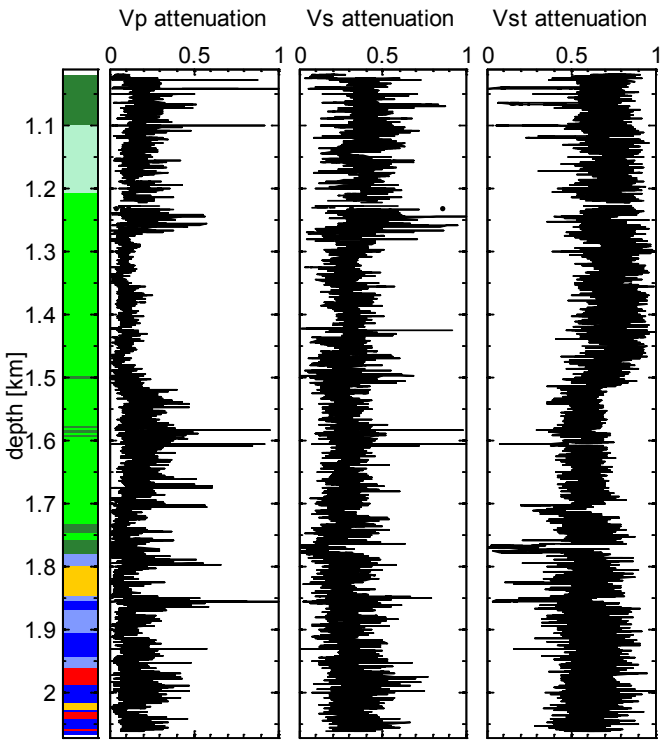

Fig. 7. Attenuation index profiles (refer to Fig. 4 for the lithology key).

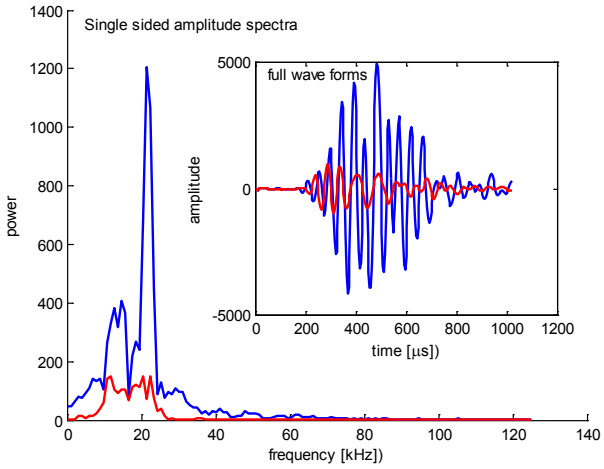

Fig. 8. Computation of frequency spectrum for a typical waveform (blue) and an attenuated waveform (red). Two parameters are extracted from the spectrum, the median frequency and the power (area below spectrum).

frequency is at 22 kHz. A secondary peak in frequency is recognizable around 15 kHz. Profiles of median frequency, power, as well as an image of the frequency content is presented on Fig. 9.

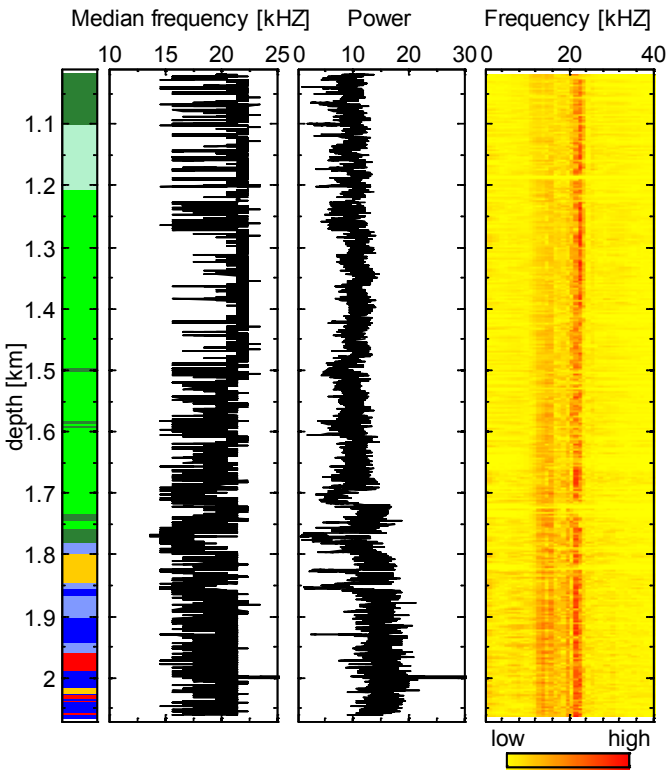

Fig. 9. Median frequency and power profiles, as well as an image of frequency content. The dominant frequency is at 22 kHz and a secondary frequency peak is recognizable around 15 kHz.

4. CORRELATION OF SONIC PARAMETERS AND ROCK PROPERTIES

4.1. Correlation of sonic parameters

The processing of the full waveforms presented above permitted the extraction of eight sonic parameters: three velocities, *Vp*, *Vs* and *Vst* from the semblance analysis, three attenuation indices *Ap*, *As* and *Ast* from the attenuation analyses and two frequency parameters, the median frequency $\tilde{f}$ and the power *P*. Prior to the assessment of the relation of these parameters with rock and rock mass characteristics, an analyses of the correlation of these sonic parameters amongst themselves was performed in order to avoid redundancy in the analyses.

The correlation between the parameters was evaluated visually on scatter plots and by computing the Pearson's linear coefficient of correlation ρ. $|\rho|$ was found to be low (less than 0.5). However some exceptions are noticeable. *Vp* and *Vs* are positively correlated, with $\rho = 0.80$. A scatter plot of *Vp* vs. *Vs* is presented on Fig. 10. The obtained compressive to shear velocity ratio are generally consistent with expected Poisson's ratio for rocks as well as within the lithology band [13].

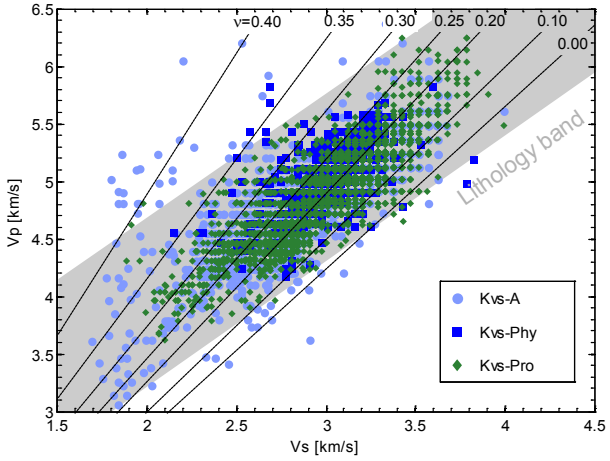

Fig. 10. Scatter plot *Vs* - *Vp* for the Kvs lithologies (the dominant lithologies in the section of the borehole under consideration).

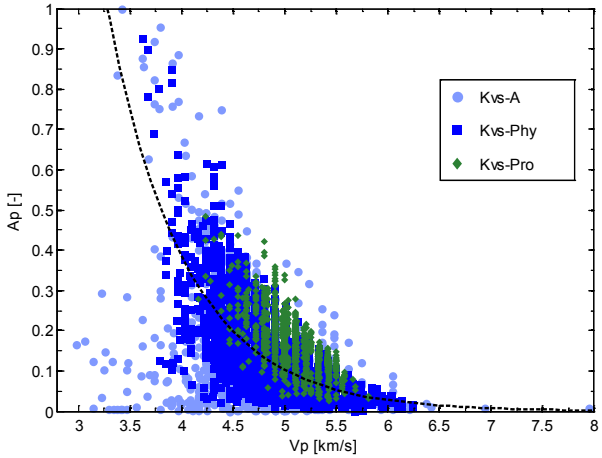

Fig. 11. Scatter plot *Vp* - *Ap* for the Kvs lithologies. The dashed line is a negative exponential best fit.

Vp and *Ap* are slightly anti-correlated with $\rho = -0.55$. A scatter plot of *Ap* and *Vp* is shown on Fig. 11. The relation between *Ap* and *Vp* is obviously not linear but follows a poorly constrained negative exponential trend.

Positive correlations with a $\rho = 0.56$ and $\rho = 0.59$ are also observed between *Ap* and *As* and $\tilde{f}$ and *P*, respectively. Also, *P* and *Ast*, although globally poorly correlated ($\rho = 0.38$), are strongly correlated for *Ap* values of less than 0.35 (see Fig. 12)

Based on these observations, correlations of sonic with rock and rock mass properties presented later will be mostly limited to non-redundant sonic parameters, i.e. *Vp* and *P*, although correlation to all computed parameters were evaluated.

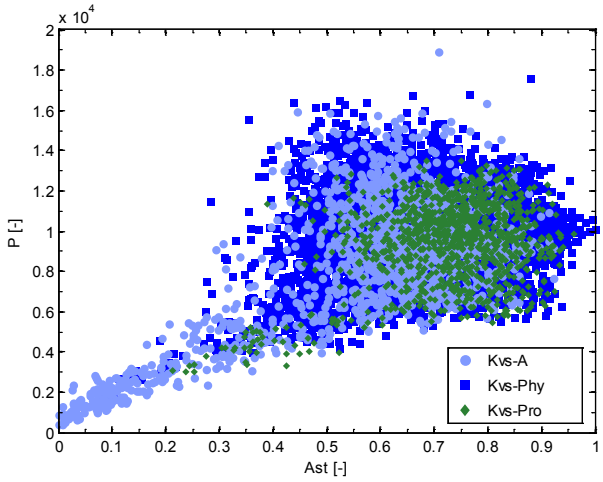

Fig. 12. Scatter plot *Ast* - *P* for the Kvs lithologies.

4.2. Correlation with intact rock properties

Following the approach generally adopted in the literature, an attempt to correlate rock strength with *Vp* is presented in the following. In a first approximation, a correlation per lithology is presented on Fig. 13. In this figure, strength data is compiled from multiple holes and includes lab derived *UCS* tests results and inferred point load index test derived *UCS values*. It provides a well supported estimation of the expected range of *UCS* for each of the lithologies. The p-wave velocities were averaged in the interval corresponding to the relevant lithologies. The mean value and standard deviation are presented in Fig. 13. The obtained ranges are consistent with the relations derived from a compilation of published data presented in Fig. 1. The velocities being generally larger than 4.5 km/s, the usage of *Vp* as a predictor for *UCS* leads to large uncertainties.

A more direct correlation of strength data and *Vp* is presented in Fig. 14. Strength data from the same hole as the sonic log are presented. Point load strength index for correlation was used over *UCS*, the later being too sparse to draw any conclusion. Also only data from the Kvs formation was available in sufficient quantity. At the depth from which point load samples were taken, the in-situ *Vp* was extracted from the sonic log parameter record and a scatter plot of point load index (Is_{50}) data vs. *Vp* was created (Fig. 14). The correlations were completed separately for Kvs-A and Kvs-Phy. No correlation was attempted on the Kvs-Pro unit because there is no evident trend (i.e. wide scatter in strength for a narrow velocity range). The correlation coefficient assuming exponential relationships are generally very low, the better being for the Kvs-A unit with a coefficient of determination, R^2=0.34. These low correlation are due to the high velocity range (>4 km/s) of the data for which correlation is known to be low (see

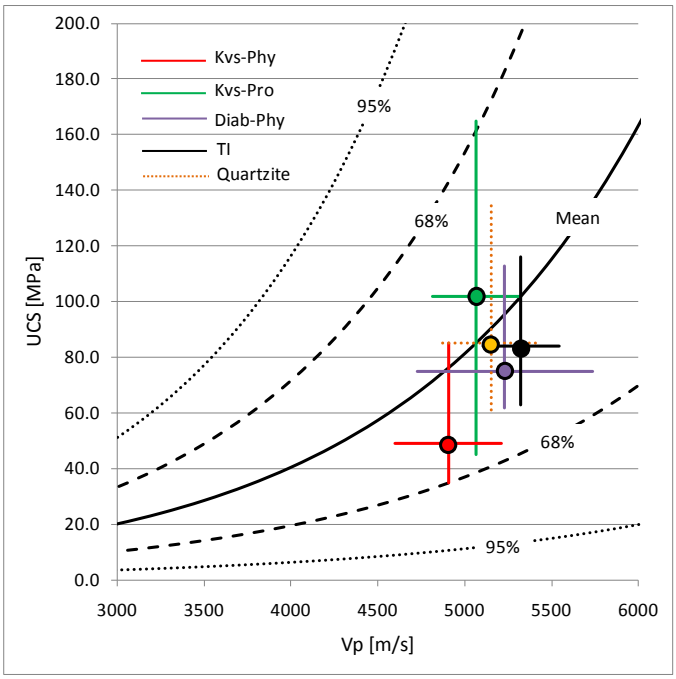

Fig. 13. Plot of p-wave velocity versus *UCS*. Solid black and dashed lines are from the published data compilation presented in Fig. 1. Crosses show the median *UCS* and mean *Vp* values. Span of vertical and horizontal lines indicate the range of data (upper and lower bounds for *UCS* and ±1 standard deviation for *Vp*). *UCS* range was obtained by compilation of *UCS* tests and interpreted point load index results from multiple boreholes in the area.

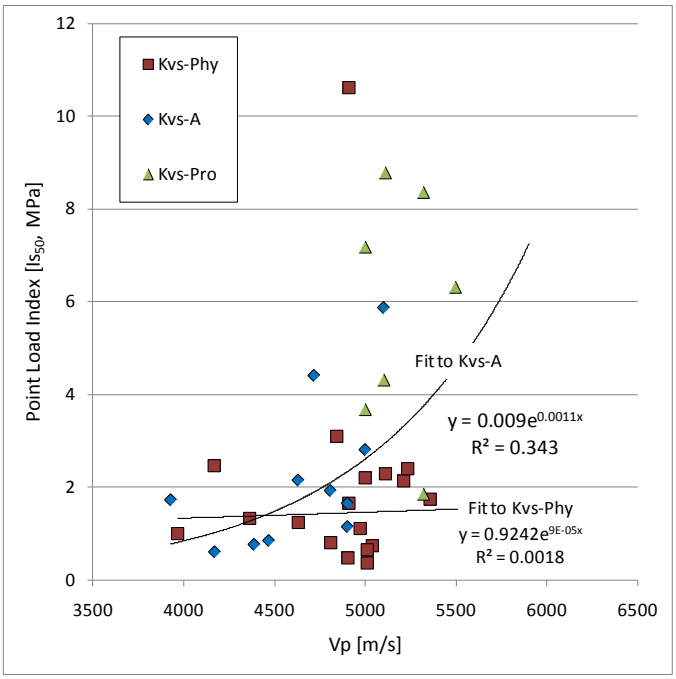

Fig. 14. Scatter plot point load index (Is_{50}) vs. *Vp* with exponential best fit curves.

Fig. 1). It is also due to the inherent variability of the point load index test results.

Further insight is gained by displaying the same data on a dual-axis plot (Fig. 15) of *Vp* versus depth and Is_{50} versus depth. This plot suggests that a correlation is not evident for the Kvs-Pro unit due to limited data (7 data points) over a small depth interval (about 100m between 1100m and 1200m downhole).

The Kvs-Phy unit displays interesting behavior between approximately 1200m and 1800m. This behavior is highlighted by the dashed arrows over the Is_{50} data points for the Kvs-Phy unit (Fig. 15 solid squares in red). There is a trend for decreasing strength with depth between 1200 m and 1700 m, followed by an increasing strength with depth between 1700 m and 1800 m. The reduction in strength is not apparent in the *Vp* data where the velocity remains fairly constant between 1200 m and 1700 m (Fig. 16). Between 1700 m and 1800 m both Is_{50} and *Vp* show increasing trends but the magnitude of the strength values obtained are not significantly greater than the Is_{50} values around 1200 m. The *Vp* values between 1700 m and 1800 m are greater than previous values, thus a higher strength should have been anticipated. It is hypothesized that these trends observed between; (1) 1200m-1700m; and (2) between 1700m-1800m; are due to the occurrence of core damage processes.

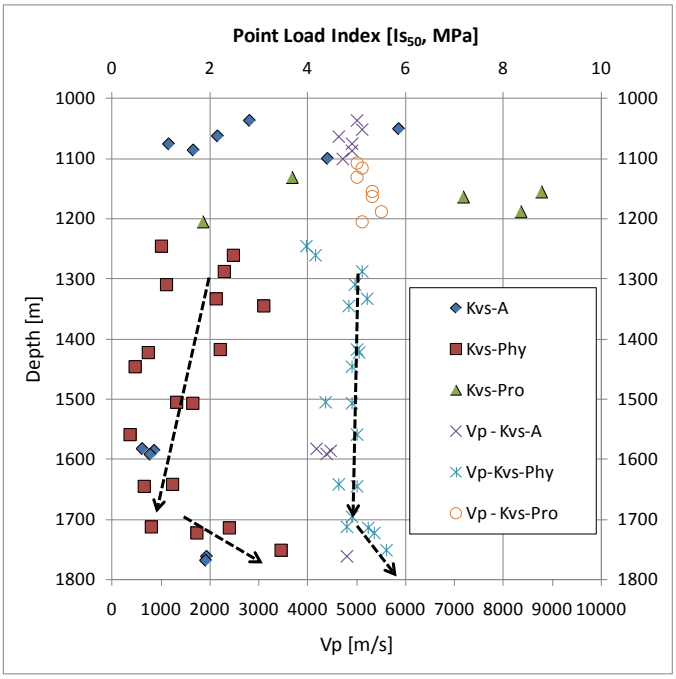

Fig. 15. Duel axis plot showing point load index (Is_{50}) versus depth (top horizontal axis) and p-wave velocity (*Vp*) versus depth (bottom horizontal axis). Dashed arrows highlight trends in the data for Kvs-Phy.

Understanding core damage is important for both mining and civil engineering projects. False indicators of low strength zones or trends as evident in the Kvs-Phy data could result in costly engineering decisions. In addition, core damage may mask higher than average strength zones that are likely between 1700m and 1800m. In this zone the Is_{50} value progresses back to values similar to those at 1200m when in actual fact, this zone is likely much stronger.

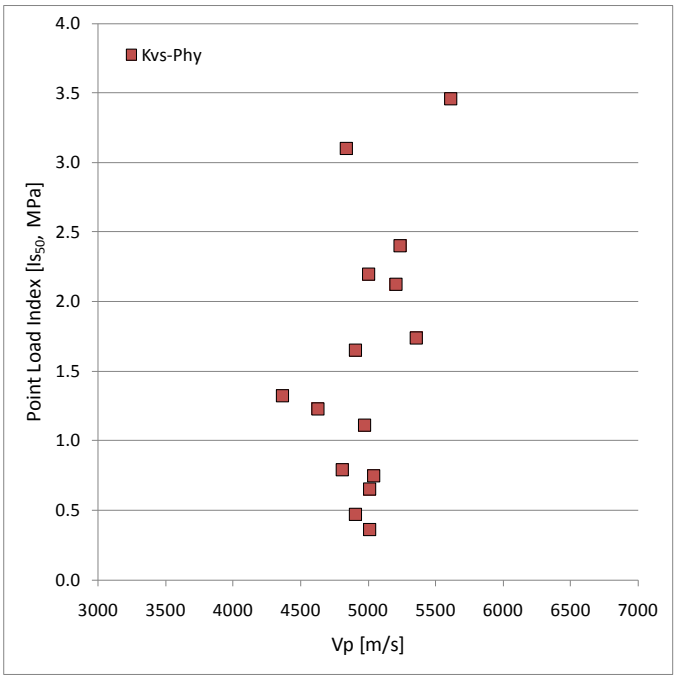

Fig. 16. Point load index (Is_{50}) versus p-wave velocity (*Vp*) for the Kvs-Phy rock unit between 1200m and 1700m showing no to little change in *Vp* for significant changes in Is_{50} suggesting core damage.

While not addressed in this article, there may be a need to correct the Kvs-Phy data for core damage. It is anticipated that the corrected data would produce a better correlation between the Kvs-Phy Is_{50} data and *Vp*.

4.3. Correlation with fracturing data

Rock mass quality was estimated from core logging parameters collected from each logging interval. A typically logging interval is 12m, but can vary depending on geology and geotechnical characteristics of the core. For each interval, parameters including RQD, open and cemented joint frequency, micro-defect density and number of joint sets were recorded. Sonic parameters were re-sampled to the rock mass quality characterization depth scale by averaging them and computing their standard deviation for each logging interval. Correlation between rock mass quality parameters and sonic parameters was then attempted. Visual evaluation using scatter plots and computation of Pearson's linear coefficient of correlation ρ indicate generally low correlation, always smaller than 0.4. An example of one scatter plot showing the open joint count vs. *P*, is presented in Fig. 17. The expected anti-correlation for these parameters, the larger number open joints inducing less sonic energy transfer, is not reflected in this plot.

The reason for this lack of correlation is hypothesized to be related to the different scale of observation: there is an order of magnitude difference between the larger

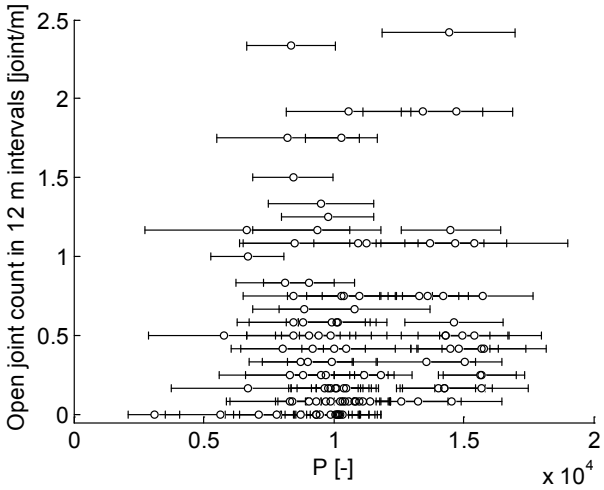

Fig. 17. Scatter plot of open joint count in 12 m windows vs. mean *P* in the same 12 m windows. Horizontal error bars cover ±1 std.

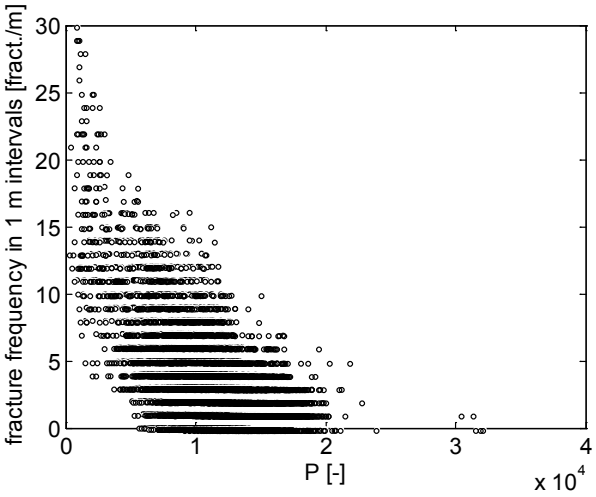

Fig. 18. Scatter plot of fracture frequency computed in 1 m intervals vs. *P*.

transmitter-receiver distance (1 m) and the rock mass quality characterization interval. To remedy this problem, an alternate approach was used: fractures were identified on an acoustic televiewer log and fracture frequency was computed within a 1 m window around each depth with a sonic record (every 10 cm). The scatter plot of fracture frequency and *P* is presented on Fig. 18. An anti-correlation is clearly identifiable, although the scatter is quite large. A similar anti-correlation exists but is less well defined between the fracture frequency and *Ast* and $\tilde{f}$ which is logical because, as shown in Section 4.1, these parameters are also correlated with *P*.

The frequency content of the full waveform is also related to fracture frequency. On Fig. 19, the amplitude

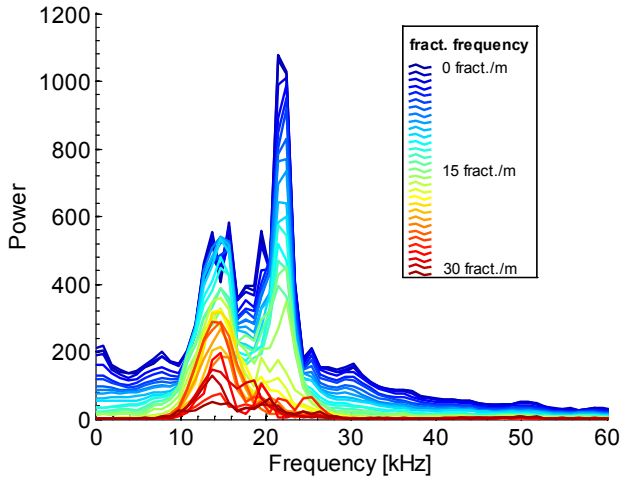

Fig. 19. Stacked frequency spectrum for borehole section with fracture frequency from 0 to 30 fractures/m.

spectra were stacked in order to obtain a representative average spectra for each fracture frequency class (from 0 to 30 fracture/m). Accompanied with the overall power decrease, a change of dominant frequency occurs from 21 kHz for rock masses with fracture frequency smaller than 10 fractures/m to 14 kHz for rock masses with higher fracture frequency.

5. CONCLUSIONS

The results presented in this paper suggest that:

- Full semblance analyses are needed to retrieve reliable *Vp* from full wave sonic wirelogs in hard rock. Simplified analyses as proposed in WellCad© lead to erroneous *Vp* estimation resulting in high *Vp* values and a broad dispersion.
- Correlation between *Vp* and strength generally exists but the scatter is very large for velocities larger than 3.5 km/s, which prevents point to point correlation. In these conditions, the direct use of *Vp* as a predictor for rock strength is not recommended. However, trends of *Vp* vs. depth plotted alongside strength with depth could be a valuable diagnostic tool to identify the occurrence of core damage and potential strength or stress anomalies..
- To investigate the correlation between sonic parameters and rock mass properties like fracturing, care must be taken to match the scale of observation. The scale of observation is determined by the emitter - receiver distance for the sonic probe and the logging interval length for core logging
- When similar scale of observation is used, a correlation between fracture frequency and attenuation is evident and accompanied also by a change of median sonic frequency to lower values. This could be used as a quick diagnostic tool for rock mass quality evaluation.

AKNOWLEDGMENTS

This research is supported by CEMI's industrial sponsors, the Government of Ontario through its Ministry of Research and Innovation and by NSERC (Natural Sciences and Engineering Research Council of Canada).

REFERENCES

1. Martin, C. D., and B. Stimpson. 1994. The effect of sample disturbance on laboratory properties of Lac du Bonnet granite. *Canadian Geotechnical Journal.* 31 (5): 692–702.
2. Eberhardt, E., D. Stead, and B. Stimpson. 1999. Effects of sample disturbance on the stress-induced microfracturing characteristics of brittle rock. *Canadian Geotechnical Journal.* 36 (2): 239–250.
3. Bahrani, N., B. Valley, and P. K. Kaiser, 2011. Discrete element modeling of Drilling-Induced core damage and its influence on laboratory properties of lac de bonnet granite. In *45th US Rock Mechanics / Geomechanics Symposium. ARMA. San Francisco*.
4. Valley, B., P. K Kaiser, and D. Duff. (2010). Consideration of uncertainty in modelling the behaviour of underground excavations. In *5th international seminar on deep and high stress mining, Santiago, Chile,* eds. Van Sint Jan, M. and Potvin, Y., 423–436. Australian Centre for Geomechanics.
5. McCann, D. M. and D. C. Entwisle. 1992. Determination of Young's modulus of the rock mass from geophysical well logs. In *Geological Applications of Wireline Logs II, Geological Society, London, Special Publications*, eds. A. Hurst, C. M. Griffiths and P. F. Worthington. 65(1): 317–325.
6. Deere, D. U. 1968. Geological Consideration, In *Rock Mechanics in Engineering Practice*. eds. Stagg, K. G. and Zienawsky, O. C. John Wiley & Sons.
7. Sharma, P. and T. Sing. 2008. A correlation between p-wave velocity, impact strength index, slake durability index and uniaxial compressive strength. *Bulletin of Engineering Geology and the Environment* 67 (1): 17–22.
8. Entwisle, D. C., P. Hobbs, L. Jones, D. Gunn, and M. Raines. 2005. The relationships between effective porosity, uniaxial compressive strength and sonic velocity of intact Borrowdale volcanic group core samples from Sellafield. *Geotechnical and Geological Engineering.* 23 (6): 793–809.
9. Kahraman, S. 2001. Evaluation of simple methods for assessing the uniaxial compressive strength of

rock. *International Journal of Rock Mechanics and Mining Sciences*. 38 (7): 981–994.

10. Kazi, A., Z. Sen, and B.-E. H. Sadagah. 1983. Relationship between sonic pulse velocity and uniaxial compressive strength of rocks. In *24th U.S. Symposium on Rock Mechanics*. 409–420.
11. Advanced Logic Technology. 2009. *WellCad software - Book 4 - FWS module*. ALT. Luxemburg.
12. Kimball, C. V. and T. L. Marzetta. 1984. Semblance processing of borehole acoustic array data. *Geophysics* 49 (3): 274-281.
13. Paillet, F. L. and C. H. Cheng. 1991. *Acoustic waves in boreholes*. CRC Press.